THE JOURNAL OF BIOLOGICAL CHEMISTRY VOL. 287, NO. 4, pp. 2328–2341, January 20, 2012
Published in the U.S.A.

ATP Hydrolysis by RAD50 Protein Switches MRE11 Enzyme from Endonuclease to Exonuclease*[S]

Received for publication, September 22, 2011, and in revised form, November 3, 2011 Published, JBC Papers in Press, November 18, 2011, DOI 10.1074/jbc.M111.307041

Jerzy Majka[‡], Brian Alford[‡], Juan Ausio[§], Ron M. Finn[§], and Cynthia T. McMurray[‡¶‖1]

From the [‡]Lawrence Berkeley National Laboratory, Life Sciences Division, Berkeley, California 94720, the Departments of [¶]Molecular Pharmacology and Experimental Therapeutics and [‖]Biochemistry and Molecular Biology, Mayo Clinic and Foundation, Rochester, Minnesota 55905, and the [§]Department of Biochemistry, University of Victoria, Victoria, British Columbia V8W 3P6, Canada

Background: RAD50-MRE11-Nbs1 complex is essential for DNA repair.
Results: ATP binding by RAD50 closes the complex; MRE11 is an endonuclease. ATP hydrolysis opens the complex; MRE11 is an exonuclease.
Conclusion: ATP hydrolysis is a switch converting MRE11 from an endonuclease to an exonuclease.
Significance: ATP-dependent nuclease switch provides a mechanism of how RAD50-MRE11 complex is able to coordinate DNA repair.

MRE11-RAD50 is a key early response protein for processing DNA ends of broken chromosomes for repair, yet how RAD50 nucleotide dynamics regulate MRE11 nuclease activity is poorly understood. We report here that ATP binding and ATP hydrolysis cause a striking butterfly-like opening and closing of the RAD50 subunits, and each structural state has a dramatic functional effect on MRE11. RAD50-MRE11 has an extended conformation in solution when MRE11 is an active nuclease. However, ATP binding to RAD50 induces a closed conformation, and in this state MRE11 is an endonuclease. ATP hydrolysis opens the RAD50-MRE11 complex, and MRE11 maintains exonuclease activity. Thus, ATP hydrolysis is a molecular switch that converts MRE11 from an endonuclease to an exonuclease. We propose a testable model in which the open-closed transitions are used by RAD50-MRE11 to discriminate among DNA ends and drive the choice of recombination pathways.

Non-homologous end joining, microhomology-mediated end joining repair, and homologous recombination pathways (HR)[2] at double strand breaks (DSBs) share a common requirement for a key early response trimeric complex comprising MRE11, RAD50, and Nijmegen breakage syndrome protein 1 (Nbs1) in humans, MRE11-RAD50-XRS2 in yeast, or dimeric RAD50-MRE11 in *Pyrococcus furiosus* (pf) (1–5). RAD50-MRE11-Nbs1 complex is essential for repair in each of these pathways. Indeed, loss of RAD50-MRE11-Nbs1 processing of double strand breaks has devastating consequences that can lead to cancer and neurodegenerative disease (1–4).

Despite its importance in recombination, the multifunctional roles of the RAD50-MRE11-Nbs1 complex in carrying out repair are poorly understood (1–3, 5, 6). During non-homologous end joining, binding of RAD50-MRE11-Nbs1 to chromosome ends prevents their degradation by processive nucleases (7–11), whereas in the HR pathway RAD50-MRE11-Nbs1 promotes DNA resection of the broken DNA ends (12–14). RAD50-MRE11 is also a component of the broad DNA replication machinery, where it plays key roles in replication fork stability and replication restart after lesion-induced fork blockage (14–18). Additionally, by interacting with either ATM or ATR kinase, the RAD50-MRE11-Nbs1 complex can activate the cell-cycle checkpoint in response to DSB or fork stalling, respectively (19–24). Thus, the RA50-MRE11-Nbs1 complex has been implicated in every aspect of DSB processing from the initial detection to the triggering signaling pathways and to the choice among pathways for repair. How this single protein complex is able to orchestrate these diverse and complex functions is unknown.

In *P. furiosus*, *RAD50-MRE11* forms a large complex comprising two subunits of the MRE11 nuclease and two subunits of RAD50 (25) that together harbor the essential DNA end recognition and nucleolytic processing functions of MRE11 (14, 25, 26). MRE11 is a 3′ to 5′ exonuclease on double strand DNA (dsDNA) and an endonuclease on single strand DNA (ssDNA) at protruding 3′ and 5′ ends and 3′ branches (27–29). At blunt ends MRE11 unwinds a few bases at the break (29), presumably to mediate 3′ to 5′ resection and promote 5′ to 3′ processing by Sae2/CtIP (2, 30–32). Sae2/CtIP interacts directly with the FHA-BRCT domains of Nbs1 (33), which recruit phosphorylated CtIP to DSBs. These steps lead to successful homologous recombination (4, 6).

At overhangs, MRE11 binds to ssDNA-dsDNA junctions in the same groove (14). The shape and extensive contacts with

* This work was supported, in whole or in part, by National Institutes of Health Grants NS40738, GM066359, NS062384, and NS060115, and CA092584 (all to C. T. M.). This work was also supported by the Mayo Foundation.
[S] This article contains supplemental sequences, Figs. S1–S5, and Tables SI–SIII.
[1] To whom correspondence should be addressed: Lawrence Berkeley National Laboratory, Life Sciences Division, 1 Cyclotron Rd., Berkeley, 94720 CA. Tel.: 510-486-6526; Fax: 510-486-6880; E-mail: ctmcmurray@lbl.gov.
[2] The abbreviations used are: HR, homologous recombination; DSB, double strand break; Nbs1, Nijmegen breakage syndrome protein 1; ATM, ataxia telangiectasia mutated; ATR, ATM- and Rad3-related; TR, Texas Red; SAXS, small angle x-ray scattering; 2-AP, 2-aminopurine; FL, full-length; pf, *P. furiosus*; AMP-PNP, adenosine 5′-(β,γ-imino)triphosphate; ATPγS, adenosine 5′-*O*-(thiotriphosphate); ss, single strand.

the DNA backbone enable two subunits of MRE11 to simultaneously contact both dsDNA and ssDNA substrates (14, 28). Thus, there is a physical basis for how MRE11 might act as a multifunctional DNA end-processing enzyme. Yet, how the MRE11 nuclease discriminates among DNA ends is not clear. *In vivo*, during DSB repair, MRE11 is needed to process DNA ends, but *in vitro* DNA recognition by RAD50-MRE11-Nbs1 has no clear biochemical preference for DNA ends, hairpin loops, or internal sites in DNA (27–29, 34).

Furthermore, the mechanisms by which RAD50 regulates MRE11 activity is poorly understood. RAD50 belongs to the structural maintenance of chromosomes family of proteins (35–39) and functions as an ABC-ATPase (40) in which RAD50 forms a composite ATP binding site comprising the N-terminal Walker A and C-terminal Walker B motifs (26, 37, 38, 41, 42) (Fig. 1*A*). The N- and C-terminal subdomains come together by intramolecular collapse of the coiled-coil domains, and ATP-induced dimerization results in sandwiching of ATP between the Walker A and B site of one monomer with the signature motif of the other monomer (37, 38).

In both *P. furiosus* and *Thermotoga maritime,* binding of the non-hydrolysable ATP analogues (AMP-PNP) to RAD50 induces a dramatic conformational rotation of the C-terminal ATPase subdomains relative to the N-terminal half in the RAD50 subunits (37, 38, 41, 42). AMP-PNP binding positions the RAD50 arms together and poises the MRE11 nuclease for wider access to DNA (14, 26, 37, 38, 41, 42), yet neither the effects of the conformational change nor the ATP dependence of the MRE11 nucleolytic functions is clear. Mutation in the ATP binding domains of RAD50 impairs HR, implying that ATP is essential to carry out MRE11 nucleolytic processing and repair (43, 44). However, the ssDNA exonuclease activity and the ssDNA endonuclease activity of MRE11 do not require ATP (27, 28), whereas the endonucleolytic cleavage of blocked DNA, dsDNA exonuclease, and 5′ dsDNA endonuclease do require ATP (27–29). The role of RAD50 ATP hydrolysis in regulating MRE11 activity remains enigmatic.

RAD50-MRE11 is a key and essential DNA processing enzyme for DSB repair, and regulation is nucleotide-driven. Despite elegant structural and molecular analyses, there is not yet a sufficiently clear picture of how nucleotide dynamics in the RAD50 subunits regulate the MRE11 nuclease activities. To address this issue, we have combined biochemical analysis, fluorescence energy transfer, and small angle x-ray scattering to evaluate nucleotide regulation and the dynamic interplay between RAD50 and MRE11. We find that ATP binding and ATP hydrolysis drive dramatic and opposing structural rearrangement in the RAD50-MRE11 complex and specify the nucleolytic activity of MRE11. ATP binding to RAD50 shifts the equilibrium to the closed conformation, conditions under which MRE11 is an endonuclease, whereas ATP hydrolysis opens the complex, conditions under which MRE11 is an exonuclease. ATP hydrolysis is a molecular switch that converts MRE11 from an endonuclease to an exonuclease.

EXPERIMENTAL PROCEDURES

Oligonucleotides—Oligonucleotides were purchased from Integrated DNA Technologies, Coralville, Iowa. All oligonucleotides were gel-purified. In anisotropy DNA binding experiments, fluorescein-labeled (6-carboxyfluorescein) DNA was used. The sequences of the oligonucleotides are presented in supplemental material.

Proteins—P. furiosus proteins and protein complexes were overexpressed and purified following a previously published procedure (25, 38).

Nucleotide and DNA Binding Assay—All binding experiments were performed at room temperature in buffer A (50 mM Tris, pH 7.5, 100 mM NaCl, 0.1% PEG-6000, 2.5% glycerol, and the indicated concentration of $MgCl_2$ and $MnCl_2$). Reactions were incubated for 10 min before measurement. Anisotropy was measured using an Infinite M1000 plate reader (Tecan Group Ltd.) at 25 °C. In nucleotide competition binding experiments, 2 nM BODIPY-labeled nucleotide was incubated with 2 μM protein (4 μM binding sites) and the indicated concentrations of "cold" nucleotide. The K_i values were calculated according to the mass-action binding model using K_D for BODIPY-labeled nucleotide obtained from a direct binding assay. All anisotropy measurements were performed in triplicate.

Cross-linking of Nucleotide and DNA Binding Assay—Experiments were performed at a concentration of 100 nM protein and 500 nM DNA. UV cross-linking of labeled nucleotides to pfRAD50 was performed in a Stratalinker 1800 (Stratagene) for 7.5 min. All binding experiments were performed at 25 °C in buffer A and the indicated concentrations of $MgCl_2$ and $MnCl_2$. Cross-linked products were resolved by SDS-PAGE, and the signals were quantified with phosphorimaging.

Fluorescence Resonance Energy Transfer (FRET)—Nucleotide binding experiments were performed at 25 °C in buffer A and the indicated concentrations of $MgCl_2$ and $MnCl_2$. Twenty-microliter reactions contained 1 μM FRET donor (BODIPY-FITC) nucleotide, 1 μM FRET acceptor (BODIPY-TR) (Texas Red (TR)) nucleotide, 1.5 μM protein (3 μM binding sites), and when applicable, 3 μM DNA. After all components were added, the reactions were incubated for 10 min before measurement. Fluorescence intensities of the FRET donor (excitation/emission 470/522 nm), FRET acceptor (excitation/emission 590/615), and FRET signal (excitation/emission 470/615) were measured using an Infinite M1000 plate reader (Tecan Group Ltd.). FRET efficiency was calculated as a ratio of the FRET signal divided by the fluorescence intensity of the donor. Data were normalized with FRET efficiency values obtained in reactions containing no protein.

Small Angle X-ray Scattering (SAXS)—SAXS data were collected at the ALS beamline 12.3.1 (Lawrence Berkeley National Laboratory, Berkeley, CA). The scattering vector is defined as $q = 4\pi\sin\theta/\lambda$, where 2θ is the scattering angle. All experiments were performed at 20 °C, and data were processed as described (45, 46). The data acquired at short and long time exposures (1 and 10 s) were merged for calculations using the entire scattering spectrum. The experimental SAXS data for different protein concentrations were measured for aggregation using Guinier plots (46). Aggregated samples were excluded from analysis. The program GNOM (46) was used to compute the pair distance distribution functions, $P(r)$. This approach also

provided the maximum dimension of the macromolecule, *D*max.

Sedimentation Velocity—Samples were dialyzed in 25 mM HEPES, pH 8.1, 100 mM NaCl, 5 mM $MgCl_2$, and 1 mM $MnCl_2$. All sedimentation velocity experiments were performed with a Beckman Optima XL-A (Brea, CA) at 20 °C. Samples were centrifuged at a rotor speed of 40,000 rpm using a two-channel centerpiece in an An-55 rotor using dialysis buffer as a reference. The absorbance of the samples was measured at 280 nm for L4-MRE11 ± ATP. The 40-base pair double-stranded DNA was tagged with fluorescein at the 5′ end. Thus, the absorbance of the DNA-containing samples was detected at 497 nm for L4-MRE11, DNA ± ATP. The sedimentation velocity data were analyzed using the enhanced van Holde-Weischet module of Ultrascan 9.9 with hydrodynamic corrections for buffers used (48).

ATPase Assay—Forty-microliter assays were performed at 55 °C in buffer A containing the indicated concentrations of $MgCl_2$ and $MnCl_2$. The assays contained 100 nM protein (200 nM ATP binding sites), 5 μM DNA, and the indicated concentrations of [α-^{32}P]ATP (0.3, 1, 3, 10, 30, 100, and 300 mM). After 1, 2, 4, 6, 10, and 15 min, 5-μl aliquots were removed from the reaction and quenched with 2 μl of 50 mM EDTA, 1% (w/v) SDS, and 20 mM concentrations each of ADP and ATP. Two microliters were spotted on a polyethyleneimine cellulose sheet and dried. The sheet was washed in water for 10 min, rinsed in ethanol, dried, and developed in 0.5 M LiCl, 1 M formic acid. The sheet was dried and subjected to phosphorimaging analysis (Bio-Rad). Rates of ATP hydrolysis were fitted to the Michaelis-Menten equation.

Exonuclease Assays—Steady state 2-aminopurine (2-AP) fluorescence 3′-5′ exonuclease assays were performed at 55 °C in buffer A containing the indicated concentrations of $MgCl_2$ and $MnCl_2$. Sixty-microliter assays contained 2 μM protein (4 μM active sites), 0.2 mM nucleotide, and the indicated concentrations of DNA substrate (1, 2.5, 5, 10, 15, and 25 μM). After 2, 4, 8, 12, and 20 min, 10-μl aliquots were removed from the reaction and quenched with 15 μl of 30 mM EDTA. Release of 2-AP from the duplex DNA was measured as an increase in fluorescence at 375 nm (excitation at 310 nm) in a Tecan Infinite M1000 plate reader. The rate of hydrolysis was calculated using free 2-AP as a standard and fitted to the Michaelis-Menten equation.

Endonuclease Assays—The endonuclease assay using oligonucleotide templates contained 2 μM MRE11 or L4-MRE11 protein, 0.2 mM nucleotide, 5 mM concentrations of both $MgCl_2$ and $MnCl_2$, and ~1 nM DNA substrate (10,000 cpm). Reactions were incubated at 55 °C for 2 h, stopped with gel loading buffer, and resolved by 12% urea-PAGE followed by phosphorimaging. For intact plasmid DNA templates, the assays contained 2 μg of ss plasmid, 1 μM full-length (FL) or L4-MRE11 protein, and 1 mM ATP incubated with 5 mM concentrations of the indicated bivalent cation. Both full-length RAD50-MRE11 and L4-MRE11 were used as indicated. Samples were taken at 0, 30, and 60 min. Disappearance of bands indicated incision.

RESULTS

Nucleotide Binding Affinity of RAD50 Is Not Affected by Its Association with MRE11—To probe the relationship between the ATP (Mg^{2+}) binding, ATP hydrolysis, and MRE11 nuclease activity, we purified three forms of RAD50 from *P. furiosus*: the full-length FL pfRAD50 (Fig. 1, *A*, *left*, and *B*) and two truncated forms of pfRAD50 (Fig. 1, *A*, *right*, *B*, and *C*). For the larger truncated forms, pfRAD50-L4 (L4) contains 25 residues of the coiled-coil domains (Fig. 1*C*, *right*), whereas in pfRAD50-L1 (*L1*) (Fig. 1*C*, *left*) only 15 residues of each coiled-coil domain are preserved (14, 37, 42). Both ends of coiled-coil helices in pfRAD50-L1 and pfRAD50-L4 are connected by a GGSGG linkers and associate with MRE11 as dimers (Fig. 1*B*). Both full-length and truncated forms of pfRAD50 form a tetrameric complex with MRE11 comprising two subunits of the MRE11 nuclease and two subunits of RAD50 (Fig. 1*D*). For our experiments, the FL protein was purified in a complex with full-length MRE11 protein. L1 and L4 were either purified alone or in a complex with a C-terminal-truncated form of the MRE11 nuclease containing the amino acids 1–381 ($MRE11_{1-381}$), which retains its nuclease activities (37). The $MRE11_{1-381}$ is insoluble in the absence of RAD50 protein, and in experiments with MRE11 nuclease alone, we used a slightly smaller, more soluble form of the protein, $MRE11_{1-342}$ (Fig. 1*B*, *lane 1*). $MRE11_{1-342}$ retains its nuclease activity; however, it is unable to bind RAD50. The purified proteins migrated on an SDS-PAGE gel according to their expected molecular weights, with no significant degradation products (Fig. 1*B*). In subsequent text, pfRAD50, pfRAD50-L1, pfRAD50-L4, and pfMRE11-RAD50-FL will be referred to as RAD50, L1, L4, and FL, respectively. $MRE11_{1-381}$, will be referred to as MRE11.

We tested whether association with MRE11 affected nucleotide affinity for wild type and mutant forms of RAD50. Nucleotide affinity was measured by fluorescence anisotropy using either labeled ATP-BODIPY-fluorescein (ATP-FITC), or ADP-BODIPY-Texas Red (ADP-TR), or ADP-FITC and ADP-TR (Fig. 1, *E* and *F*). *P. furiosus* is a widely used extremophile that optimally grows at 55 °C, and RAD50-MRE11 in this organism is inactive at 25 °C (25). Thus, in these experiments binding was performed at 25 °C to prevent ATP hydrolysis in the RAD50 subunits during the measurements. ATP and ADP binding to RAD50 required Mg^{2+} or Mn^{2+} as structural co-factors (Table 1) (14, 27, 28), and in their absence nucleotide binding was not measurable (Table 1). However, nucleotide affinity for FL, L1, or L4 or their complexes with MRE11 was not significantly different whether Mg^{2+} or Mn^{2+} was added independently or in a stoichiometric mixture (Table 1). Nucleotide affinity was also unaffected when L4 or L4-MRE11 was bound to either ssDNA or dsDNA (Fig. 1*E*, supplemental Table SI). Under all conditions, affinity was modest (around 1 μM) (Table 1).

As a second approach, we measured the affinity of nucleotide binding for FL, L1, L4, or their complexes with MRE11 using UV cross-linking. However, ATP and ADP dissociated rapidly from RAD50 (Fig. 1*G*, supplemental Fig. S1*A*), and cross-linking of ATP or ADP to FL, L1, or L4 was weak (Fig. 1*H*, *lanes 2–6*, supplemental Fig. S1*B*) relative to a control ABC-ATPase, human MutS-β (MSH2-MSH3) (49, 50) (Fig. 1*H*, *lane 1*,

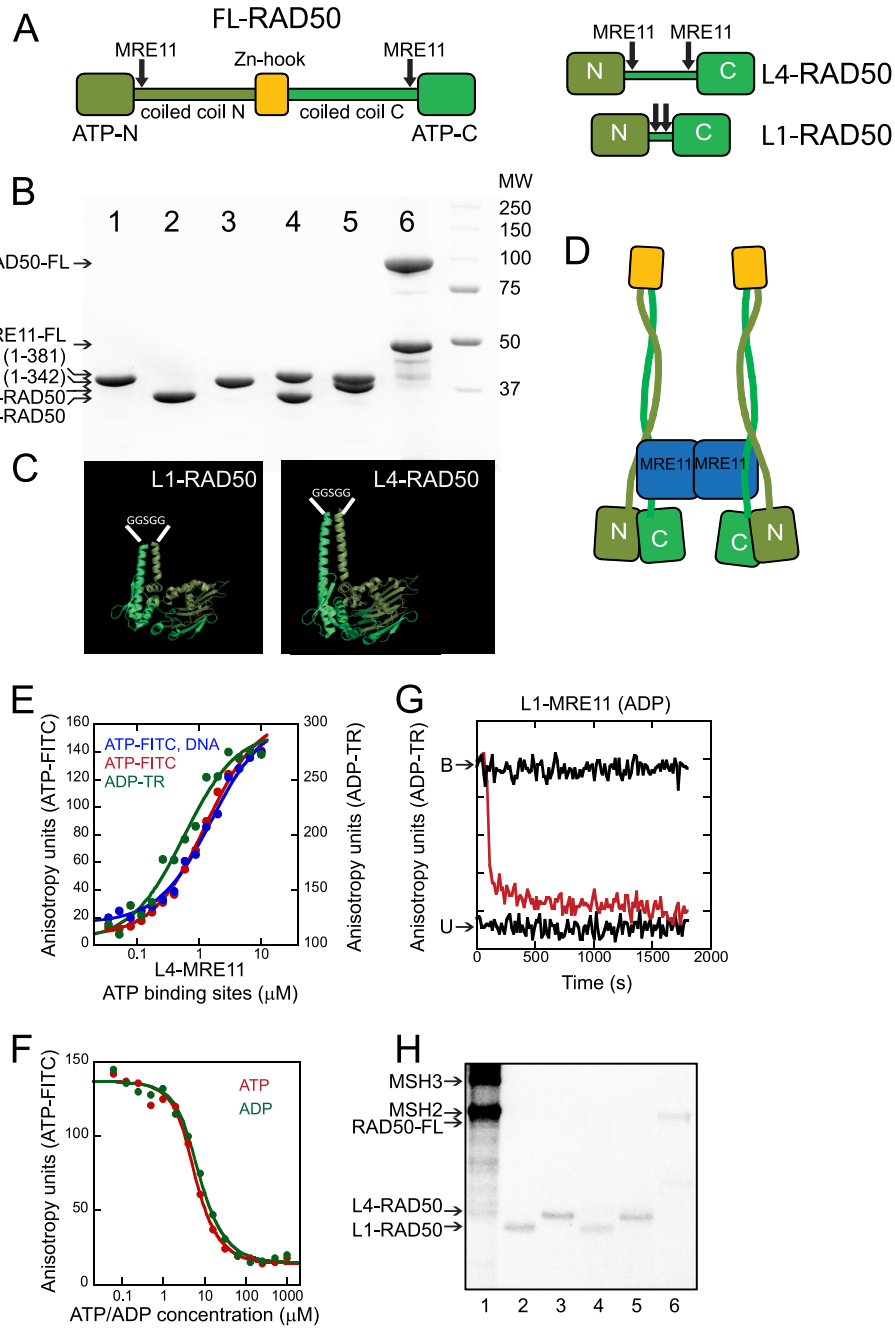

FIGURE 1. **Nucleotide binding to purified pfRAD50s and to their complexes with MRE11.** *A*, linear representation of the FL pfRAD50 is shown. The MRE11 binding sites are indicated by the *arrows*, the zinc hook region is in *gold*, and the N- and C-coiled coil domains are *dark* and *light green*, respectively. The ATP binding sites (*ATP N* and *C*) are indicated. *Right*, linear representations of the truncated forms of RAD50 are shown. L4-RAD50 (*L4*) and L1-RAD50 (*L1*), each of which contains MRE11 binding sites, are shown. *B*, shown is SDS-PAGE resolution of the purified forms of pfRAD50 and pfMRE11 proteins used in the experiments. *1*, $MRE11_{1-342}$; *2*, L1-RAD50; *3*, L4-RAD50; *4*, L1-$MRE11_{1-381}$; *5*, L4-$MRE11_{1-381}$; *6*, FL-RAD50 and FL-MRE11. *C*, shown are pMOL images of the engineered L1-RAD50 and L4-RAD50 indicating the peptide linker (GGSGG) (*white*). *D*, shown is a schematic representation of the FL MRE11-RAD50 heterodimer. *E*, binding of BODIPY-labeled nucleotides for either ATP-FITC (*red*) or ADP-TR (*green*). Reactions containing DNA are indicated in *blue*. L4-MRE11 at the indicated protein concentration (expressed as concentration of ATP binding sites) was incubated at 25 °C for 5 min with 5 nM nucleotide in a 20-μl reaction volume. In the DNA binding curve (*blue*), the reactions contained 5 μM 40-bp double-stranded oligonucleotide. Anisotropy was measured on a TECAN plate reader using excitation and an emission wavelength of 470 and 522 nm for ATP-FITC and 590 and 615 nm for ADP-TR. Data were fitted (*solid lines*) to a Langmuir isotherm. *F*, in competition experiments, unlabeled nucleotide was added at the indicated concentrations to 3 μM L4-MRE11 (6 μM ATP binding sites) pre-bound with 5 nM ATP-FITC (*red*) or ADP-TR (*green*). *G*, displacement kinetics of prebound ADP-TR from pfRAD50 were measured using unlabeled ADP as a competitor. *B* indicates bound ADP-TR in the absence of nucleotide, and *U* indicates unbound pfRAD50. *H*, protein products of UV-cross-linking with labeled nucleotides is shown. *1*, MSH2-MSH3 control; *2*, L1; *3*, L4; *4*, L1-MRE11; *5*, L4-MRE11; *6*, FL. Reactions contained 100 nM concentrations of the indicated protein and 500 nM nucleotide. UV cross-linking of labeled nucleotides to RAD50 was performed in a Stratalinker 1800 cross-linker (Stratagene) for 7.5 min, and the products were resolved by SDS-PAGE.

supplemental Fig. S1). Thus, nucleotides bound to the RAD50 subunits were not retained in the ATP binding sites but rapidly exchanged with solution nucleotides.

To ensure that the fluorescence analogues did not reduce affinity or promote rapid nucleotide dynamics, we measured the K_i for competition of ATP-FITC and ATP-TR with other

TABLE 1
Rad50 Nucleotide affinities measured by fluorescence anisotropy
ND, not determined.

	$K_{D,ATP}$	$K_{D,ADP}$	$K_{I\text{-}ATP,ATP}$	$K_{I\text{-}ATP,ADP}$
	μM	μM	μM	M
L1				
Mg^{2+}	1.51 ± 0.20	0.835 ± 0.23		
Mn^{2+}	1.45 ± 0.16	1.67 ± 0.66		
No^{2+} ion	ND	ND		
L4				
Mg^{2+}	1.94 ± 0.10	0.254 ± 0.043	4.1 ± 0.40	1.5 ± 0.24
Mn^{2+}	2.46 ± 0.18	0.646 ± 0.19	5.7 ± 0.90	2.0 ± 0.30
No^{2+} ion	ND	1.53 ± 0.41		
L1-MRE11				
Mg^{2+}	1.86 ± 0.26	0.510 ± 0.089		
Mn^{2+}	1.33 ± 0.19	0.840 ± 0.20		
No^{2+} ion	ND	ND		
L4-MRE11				
Mg^{2+}	1.05 ± 0.12	0.260 ± 0.051	1.1 ± 0.20	1.9 ± 0.28
Mn^{2+}	0.853 ± 0.063	0.280 ± 0.069	0.9 ± 0.13	1.0 ± 0.15
No^{2+} ion	ND	ND		
FL				
Mg^{2+}	1.61 ± 0.37	0.328 ± 0.083		
Mn^{2+}	1.01 ± 0.41	0.297 ± 0.12		
No^{2+} ion	ND	ND		

nucleotides. We found that K_D for binding of ATP-FITC (Mg^{2+}) and the K_i for its inhibition by unlabeled ATP (Mg^{2+}), non-hydrolysable ATP analogues ATPγS (Mg^{2+}), or the transition state analog ADP-BeF_n (Mg^{2+}) were similar (supplemental Fig. S2, Table 1). Thus, the nucleotide binding to L4 and L4-MRE11 in solution was reversible (Table 1). Collectively, these findings revealed that nucleotide affinity for FL, L1, or L4 was remarkably unaffected by either the structure or function of the RAD50 subunits. Nucleotide affinity for RAD50 was the same whether or not it was associated with MRE11 whether the RAD50 ATPase (Mg^{2+}) or whether the MRE11 nuclease (Mn^{2+}) was active, or RAD50 was bound to DNA (Fig. 1*E*, supplemental Table SI). Thus, RAD50 did not significantly contribute to the regulation of MRE11 at the level of nucleotide or DNA affinity.

RAD50 Is Double-occupied with ATP Both On and Off DNA—As judged by the crystal structure, binding of two AMP-PNP molecules induces dimerization of the head domains and a dramatic structural change that closes the RAD50-MRE11 complex (38, 42). However, in solution we found that AMP-PNP was a poor competitor for ATP-FITC bound in the L4 subunits (supplemental Fig. S2). Thus, we tested whether nucleotide occupation altered the structures of L1, L4, or their complexes with MRE11 when reversible ATP analogues were added in solution, and whether the alterations depended on DNA binding.

In the first experiments we tested whether ATP occupied one or two of the ATP sites in L4. RAD50 was incubated with an equal concentration of ATP-FITC (as a donor) and ATP-TR (as an acceptor), and we tested whether nucleotide addition resulted in FRET at 25 °C, conditions under which ATP hydrolysis in L4 is inactive (Fig. 2, *A* and *B*). If two composite Walker sites were occupied with ATP in solution, then we anticipated a FRET signal. Indeed, a strong FRET signal was observed for L4 and its complexes with MRE11 when ATP-FITC and ATP-TR were added together (Fig. 2*B*). The FRET signal increased as the ATP binding sites were filled and diminished as the excess protein competed for the donor and acceptor nucleotides (Fig. 2*A*). However, in all cases, the maximum FRET signal occurred at a 1:1 ratio of nucleotide per RAD50 binding site, indicating that both sites were occupied equally (*starred bars*, in Fig. 2, *A* and *B*).

In our nucleotide binding experiments (Fig. 1, *E* and *F*), the best fit of experimental data to the Langmuir isotherm did not deviate from a theoretical curve, implying that ATP binding to the RAD50 subunits was not cooperative. Thus, in solution the RAD50 dimer bound two ATP nucleotides in close proximity in the presence or absence of MRE11 (Fig. 2, *C* and *D*), and nucleotide binding to one subunit did not influence nucleotide binding to the other subunit. The strong FRET signal induced by ATP binding to L4 and L4-MRE11 did not depend on the presence of DNA, indicating that both complexes existed in solution primarily in a double-occupied state (Fig. 2, *E–G*).

Binding of Two ATPs Promotes "Open" and "Closed" Conformations of RAD50 and RAD50-MRE11 Complexes—The FRET signal observed after binding of ATP (Mg^{2+}) to L4 and L4-MRE11 provided evidence that the RAD50 subunits of L4-MRE11 moved closer together. Indeed, we found that ATP-bound L4-MRE11 formed a closed structure which exceeded that expected of simple dimerization (Fig. 2*D*). Both L1 and L4 (Fig. 1) dimerize (37, 38), yet we were unable to observe a FRET signal between ATP-FITC and ATP-TR when bound to L1, and the FRET signal for L1-MRE11 was weak (Fig. 2*B*, supplemental Fig. S3). The lack of a FRET signal for the nucleotide-bound L1 complex was not due to differences in nucleotide affinity (Table 1). Nucleotides bound equally well to L1 and L4 or their complexes with MRE11, and the K_i for competition with unlabeled ATP was similar to the K_D for ATP-FITC and ATP-TR binding to L1 (Table 1). The observations implied that in solution as well as in the crystal structure (41, 42), binding of ATP to L4 and L4-MRE11 induced a closed complex that required the coiled-coil domain of RAD50.

In solution, however, ATP (Mg^{2+}) binding to RAD50 was necessary but not sufficient for closure. In the absence of ATP

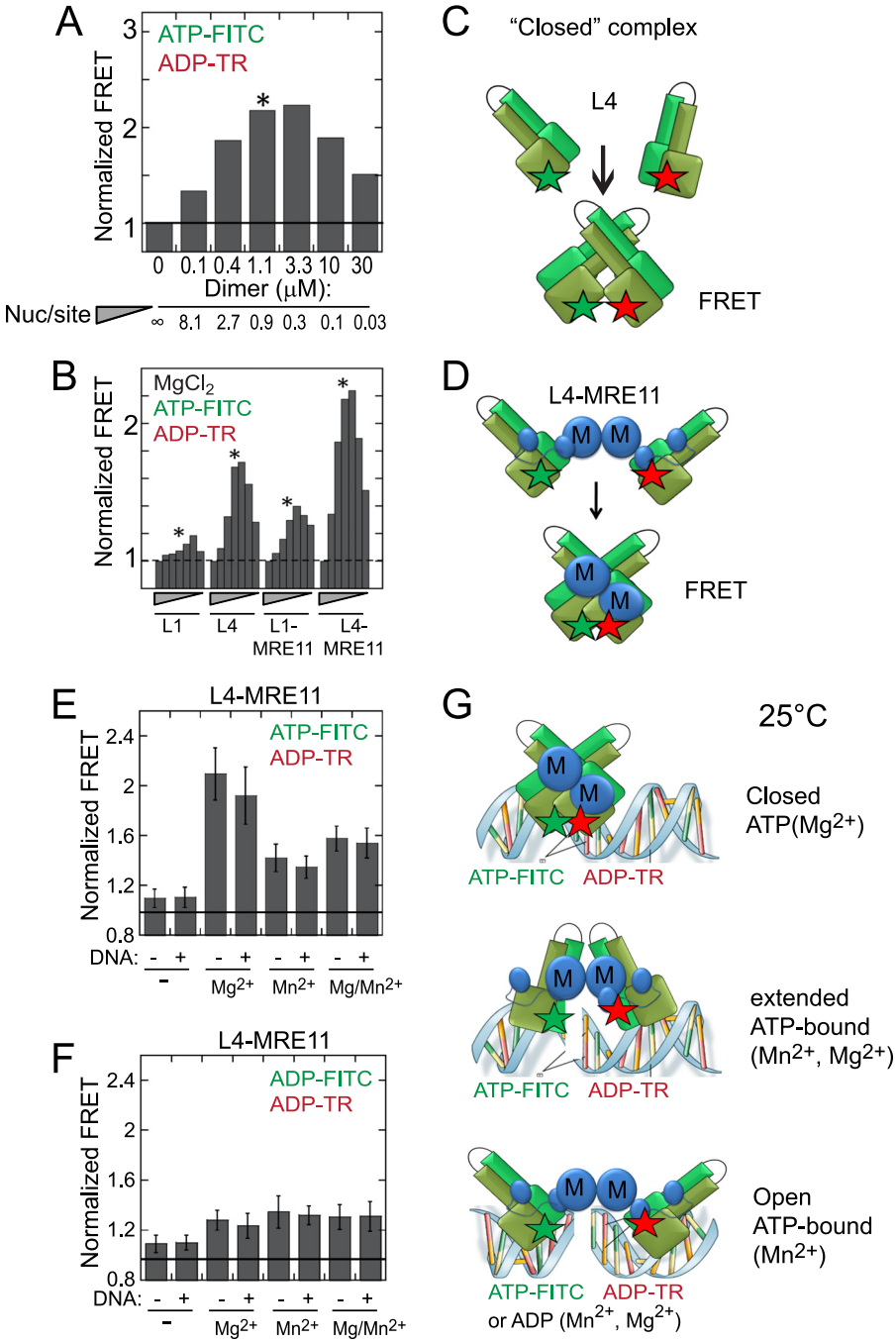

FIGURE 2. **ATP binding closes both RAD50 and RAD50-MRE11 complexes.** *A* and *B*, the normalized FRET signal for ATP-bound L1, L4, or their complexes with MRE11 is shown. *A*, an example of the normalized FRET analysis is shown. In the assays each BODIPY-labeled nucleotide was held constant at 1 μM, and purified protein (expressed as dimers) was added in increasing concentrations. As protein concentration increases, the nucleotide per site ratio decreases as indicated by the inverted *triangles*. The *star* indicates that the maximum FRET intensity occurred at a nucleotide per binding site ratio of ~1:1. *B*, shown is the FRET analysis in *A* for ATP-FITC and ATP-TR binding to L1, L4, L1-MRE11, or L4-MRE11 protein in the presence of Mg^{2+}. Reactions containing purified protein, nucleotides, and 5 mM $MgCl_2$ were incubated in a 20-μl reaction volume for 5 min at 25 °C before measurement. *C* and *D*, shown is a schematic diagram of the ATP-driven closed complexes derived from the FRET results for L4 (*C*) and L4-MRE11 (*D*). The *green* and *red stars* are the ATP-FITC- and ATP-TR-labeled nucleotides, respectively. *M* (*blue*) is MRE11; *light* and *dark green* dimer is RAD50. *Close stars* indicate FRET, whereas the *separated stars* represent no FRET. The fluorescence intensity of a donor (excitation 470 and emission 522 nm) and intensity of energy transfer (excitation 470 and emission 615 nm) were recorded in a TECAN plate reader. *E*, shown are FRET results of *B* in which 5 mM ATP (Mg^{2+}), ATP (Mn^{2+}), a stoichiometric ratio of both, or no ion (−) were added to the L4 or L4-MRE11 in the presence (+) or absence (−) of DNA (40-bp double-stranded oligonucleotide). *F*, details are the same as *E* except that ADP-FITC and ADP-TR were the added nucleotides. *G*, shown is a schematic diagram for the RAD50-MRE11 complexes derived from the FRET results depicting the conformation of ATP-bound complexes. *Top*, the L4-MRE11 complex is closed when RAD50 is bound with ATP (Mg^{2+}); *bottom*, complex is open when L4-MRE11 is bound with ATP (Mn^{2+}) or ADP (in the presence of any added divalent ion); *middle*, an intermediate conformation or mixture when L4-MRE11 is bound equally with ATP (Mg^{2+}) and ATP (Mg^{2+}). *Red* and *green stars* represent ATP-TR- and ATP-FITC-labeled nucleotide, respectively.

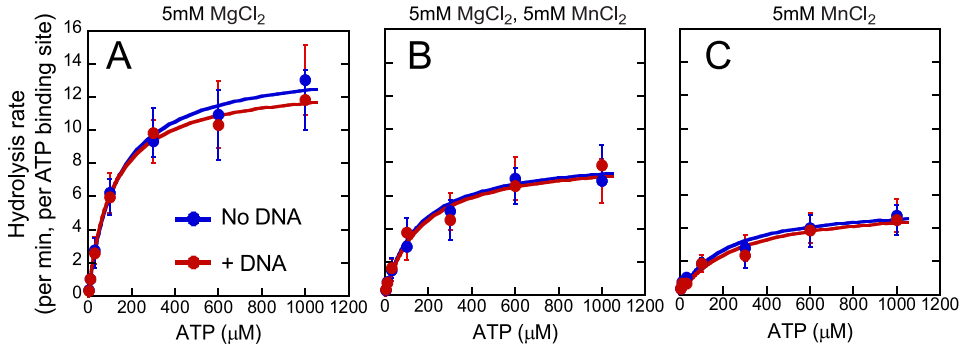

D

	$MgCl_2$		$MgCl_2$, $MnCl_2$		$MnCl_2$	
	K_M (μM)	k_{cat} (min^{-1})	K_M (μM)	k_{cat} (min^{-1})	K_M (μM)	k_{cat} (min^{-1})
No DNA	135 ± 19	14.1 ± 0.54	166 ± 34	8.30 ± 0.51	209 ± 72	5.48 ± 0.61
+ DNA	113 ± 13	12.9 ± 0.38	159 ± 52	8.45 ± 0.82	256 ± 107	5.43 ± 0.79

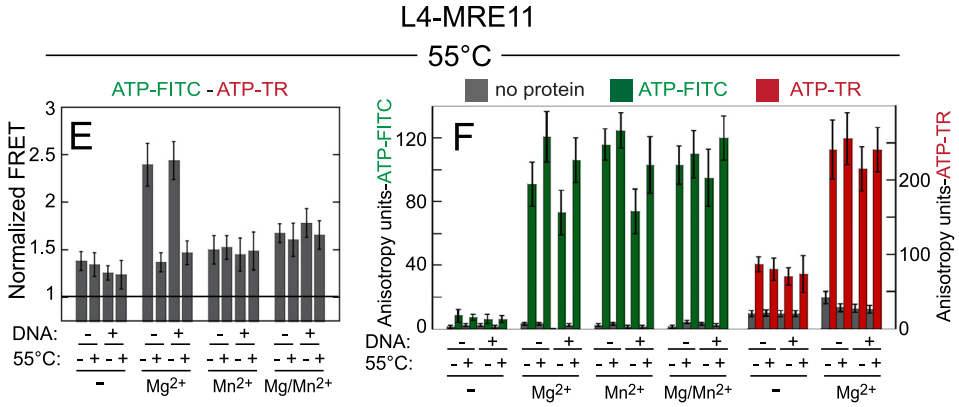

FIGURE 3. **ATP hydrolysis opens the RAD50-MRE11 complex.** *A–C*, ATPase assays were performed at 55 °C. L4-MRE11 was added to nucleotides with (*red*) or without (*blue*) DNA (5 μM 40-bp double-stranded oligonucleotide) and incubated for 10 min at 55 °C. At 2, 4, 6, 10, and 20 min, 5-μl aliquots were removed, quenched, and analyzed by TLC. Data were fit (*solid lines*) to a Michaelis-Menten equation. Each reaction contained the indicated ion or combination of ions, 2 μM L4-MRE11 (4 μM ATP binding sites), and the indicated concentrations of [α-^{32}P]ATP. *D*, the percentage of ADP formed was quantified by phosphorimaging and used to calculate ATP hydrolysis rates (expressed in turnover number per minute) in the presence or absence of DNA. *E*, shown is FRET between ATP-FITC and ATP-TR bound to L4-MRE11 at 55 °C in Mg^{2+}, Mn^{2+}, or a stoichiometric ratio of both Mg^{2+}/Mn^{2+}, or no ion was measured as described in Fig. 2. ATP hydrolysis and/or the addition of Mn^{2+} is sufficient to lose FRET and open the closed complex. *F*, shown is the nucleotide binding affinity measured at 55 °C for reactions in *E* using fluorescence anisotropy for ATP-FITC and ATP-TR. The excitation and emission of wavelengths were 470 and 522 nm for ATP-FITC and 590 and 615 nm for ATP-TR; *gray* is no protein, the *green bar* is ATP-FITC, and the *red bar* is ATP-TR. The presence (+) or absence (−) of DNA is indicated. Samples in the presence (+) or absence (−) of heating to 55 °C are indicated.

hydrolysis (25 °C), both on or off DNA, a FRET signal for ATP-bound RAD50-MRE11 was lost in the presence of Mn^{2+} relative to Mg^{2+} added alone (Fig. 2*E*, supplemental Fig. S3). Furthermore, the FRET signal for the ATP-bound complex was intermediate between the signal for ATP (Mg^{2+}) or ATP (Mn^{2+}) if the two were added together. Thus, multiple ATP-bound forms of L4-MRE11 were present in solution and ranged from closed to open depending on the added ion (Fig. 2*G*): closed complexes (in Mg^{2+}), open complexes (in Mn^{2+}), and an extended state and/or mixtures of the closed and open complexes ($Mg^{2+}$and Mn^{2+}).

ATP Hydrolysis Opens Closed Complex—We tested the consequences of ATP hydrolysis on the structural conformation of the L4-MRE11. At 25 °C, the FRET signal was consistently lost when ATP-FITC and ADP-TR (supplemental Fig. S3) or ADP-FITC and ADP-TR (Fig. 2*F*) were used as FRET pairs, suggesting that ATP hydrolysis might drive the opening of ATP-bound RAD50-MRE11. To test this hypothesis, we measured the hydrolytic activity of RAD50-MRE11 at 55 °C (the temperature optimum for the catalytic activity of pfRAD50) side by side with the FRET intensity of the complex. The rate of ATP hydrolysis was derived from the level of conversion of ATP to ADP after their resolution using thin layer chromatography (TLC) (Fig. 3, *A* and *D*). As expected, at 55 °C, ATP hydrolysis in the L4-MRE11 complex was active in the presence of Mg^{2+} (Fig. 3, *A* and *D*), whereas little activity was observed when the added ion was Mn^{2+} (required for MRE11 nuclease activity) (Fig. 3, *C* and *D*). Mn^{2+} competed with Mg^{2+} for binding to RAD50 but failed to support significant ATP hydrolytic activity. Consequently, the rate of ATP hydrolysis was intermediate between Mg^{2+} and Mn^{2+} when both ions were present (Fig. 3, *B* and *D*).

We correlated the ATPase activity of RAD50 with changes in FRET intensity. Remarkably, when L4 or L4-MRE11 was incubated with ATP (Mg^{2+}) for 10 min at 55 °C, the FRET signal

diminished to the base value, indicating that the L4 dimer was in close proximity before but not after ATP hydrolysis (Fig. 3*E*). Thus, in the absence of nuclease activity, ATP hydrolysis alone was capable of opening the closed L4-MRE11 complex. Loss of the FRET intensity could arise if either the donor or acceptor nucleotides dissociated upon heating. Thus, in parallel reactions we measured nucleotide binding of both the TR- and the FITC-labeled nucleotides by anisotropy at their distinct λ_{max} (Fig. 3*F*). Binding of the ATP analogues was not significantly different from L4-MRE11 before and after heating under physiological ionic strength. ATP binding to L4-MRE11 (supplemental Fig. S3) was specific because, as expected, little to no nucleotide bound to L4 (supplemental Fig. S3) or to L4-MRE11 (Fig. 3*F*, Table 1) in the absence of added ions. Thus, the loss of FRET was due to hydrolysis-driven separation of the RAD50 subunits.

The FRET intensity of L4-MRE11 was low before or after heating when both the RAD50 ATPase and the MRE11 nuclease were active simultaneously (Mn^{2+} and Mg^{2+} together). However, at 55 °C the FRET intensity of L4-MRE11 was consistently higher relative to either ATP (Mn^{2+}) or to ATP (Mg^{2+}) added alone (Fig. 3*E*). Because the rate of ATP hydrolysis in Mn^{2+} and Mg^{2+} is slower relative to Mg^{2+} alone, the results implied that ATP hydrolysis modulated the extent of opening of the nuclease active L4-MRE11, which was in an intermediate conformation between a fully closed and a fully open state when both L4 and MRE11 were active enzymes.

The Open Configuration of RAD50-MRE11 Binds Best to DNA—We asked whether the open and closed conformations differed when L4-MRE11 was bound to DNA. However, for all measurements tested, we were unable to observe a conformational difference in the DNA-bound and DNA-free RAD50-MRE11 complexes. Using SAXS (45), the addition of ATP (Mg^{2+}) resulted in a more "bumpy" scattering curve and a sharper $P(r)$ function maximum, consistent with a more compact, spherical conformation of the closed complex (Fig. 4*A*). However, the ATP-dependent conformational changes of the DNA-free and DNA-bound complexes were indistinguishable (Fig. 4*B*). Sedimentation velocity analysis (51, 52) confirmed that the addition of ATP (Mg^{2+}) to DNA-bound L4-MRE11 was characterized by an increase in the $s_{20,w}$ value from 8.0 to 8.5 (Fig. 4*D*), but the analogous alteration was observed upon ATP binding to L4-MRE11 in the absence of DNA (Fig. 4*C*). Additionally, the rate of ATP hydrolysis in the RAD50 subunits of L4-MRE11 was equivalent in the presence or absence of DNA (Fig. 3), implying that opening of the closed complex occurred equally well under both conditions. No differences in the FRET signal of the DNA-bound (Fig. 2, *E* and *F*) and DNA-free L4-MRE11 (supplemental Fig. S3) were observed under any of the conditions measured. Thus, RAD50 acted as an autonomous unit in which opening and closing resulted from continuous cycles of ATP binding, ATP hydrolysis, and ATP exchange whether or not L4-MRE11 was bound to DNA.

Because the presence of DNA did not influence the structural transition, we tested whether the structural transition altered the affinity for DNA for the RAD50-MRE11 complex (Fig. 4, *E* and *F*). We added purified L4 or L4-MRE11 to FITC-labeled ssDNA or dsDNA and measured the DNA binding affinity under conditions of Mg^{2+} (closed configuration) or Mn^{2+} (open configuration). These experiments were performed at 25 °C to silence enzymatic activity of RAD50-MRE11 (49). In agreement with previous results (14, 25, 27, 28, 38), we found that both L4 and MRE11 were able to bind DNA (supplemental Table SII). However, the open and closed L4-MRE11 complexes had significantly different DNA affinities. For L4, at 25 °C DNA binding affinity was modest and did not change whether L4 was bound with ATP or whether Mg^{2+} or Mn^{2+} were the added ions (supplemental Table SII). In contrast, DNA binding affinity of MRE11 and L4-MRE11 substantially increased (10–20-fold) in the presence of Mn^{2+} (Fig. 4, *E* and *F*, supplemental Table SII). The increase in DNA binding affinity of L4-MRE11 was observed whether Mn^{2+} was added independently or together with Mg^{2+} (supplemental Table SII). Thus, RAD50-MRE11 bound best to DNA in the presence of Mn^{2+}, conditions under which the complex was open (Fig. 2, *E* and *F*).

ATP Hydrolysis Prevents Loss of MRE11 3′ to 5′ Exonuclease Activity—MRE11 is a 3′ to 5′ exonuclease on dsDNA and an endonuclease on ssDNA at protruding 3′ and 5′ ends and 3′ branches (27–29). Because L4-MRE11 could form open and closed states when bound to DNA, we tested whether the different structural states had consequences on the nuclease functions of the MRE11.

To directly measure the exonuclease activity of MRE11, we synthesized a DNA duplex in which a 2-AP base was incorporated at the second position from the 3′ end of the DNA duplex (Fig. 5*A*) (14). The 2-AP is intrinsically fluorescent, but its fluorescence is quenched when incorporated in dsDNA (Fig. 5*A*). If the MRE11 exonuclease was active, then we anticipated a gain in fluorescence intensity when 2-aminopurine is released during 3′ to 5′ nucleolytic activity. At 55 °C in the presence of Mn^{2+} added alone (Fig. 5*B*) or together with Mg^{2+} (Fig. 5*D*), $MRE11_{1-342}$ excision resulted in efficient release of 2-AP. $MRE11_{1-342}$ does not bind ATP, and as expected, catalytic activity of $MRE11_{1-342}$ was not significantly affected by the addition of ATP, ADP, or the non-hydrolyzable analog ATPγS (Fig. 5, *B* and *D*).

We repeated the MRE11 exonuclease assay for the L4-MRE11 complex. Indeed, when associated with RAD50, MRE11 was an active exonuclease in the absence of nucleotides as long as Mn^{2+} was added to the reaction (Fig. 5, *C* and *E*). Surprisingly, the presence of RAD50 markedly suppressed the specific activity of MRE11 exonuclease activity (k_{cat}/K_m) (supplemental Table SIII) around 2-fold relative to MRE11 alone (compare Fig. 5, *B* and *C*, supplemental Table SIII). Furthermore, the exonuclease activity of L4-MRE11 in the presence of ATP (Mn^{2+}), ATPγS (Mn^{2+}), or ADP (Mn^{2+}) was not substantially different from that observed in the absence of nucleotide (Fig. 5*C*). These findings implied that RAD50 intrinsically inhibited the exonuclease activity of L4-MRE11, and in the absence of ATP hydrolysis, exonuclease suppression was independent of bound nucleotide.

We tested the effects on the MRE11 exonuclease activity if RAD50 was also an active ATPase (ATP (Mg^{2+} and Mn^{2+})) (Fig. 5*E*). However, we observed only a modest rise in the exo-

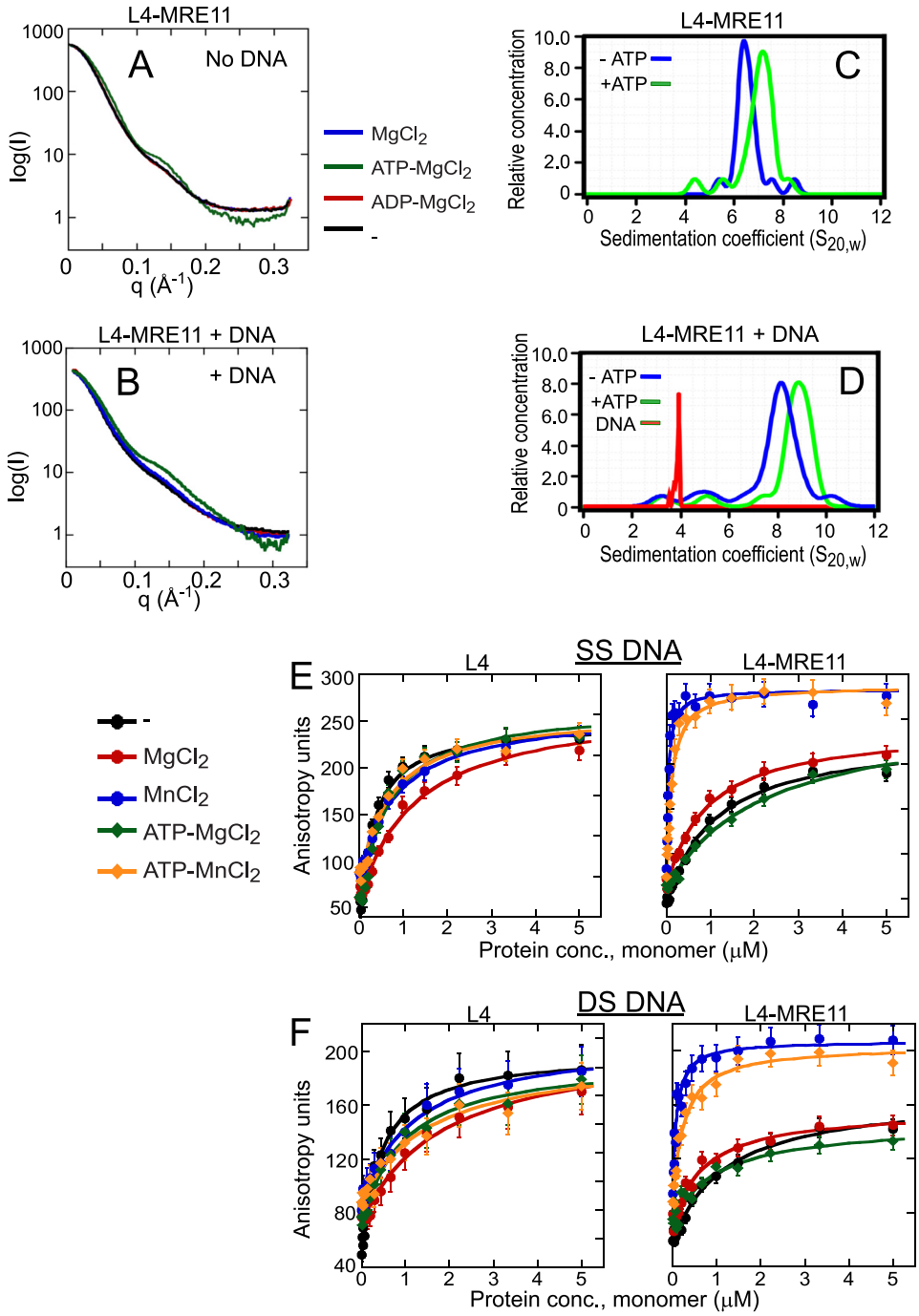

FIGURE 4. **DNA binding does not influence the conformation of L4 and L4-MRE11.** *A* and *B*, SAXS of the L4-MRE11 heterotetramer (*A*) or the L4-MRE11 heterotetramer (*B*) in the presence of DNA in reactions containing (25 μM) protein and no ion (*black*), no nucleotide (*blue*), 200 μM ADP (Mg^{2+}) (*red*), or 200 μM ATP (Mg^{2+}) (*green*). The plot is of log intensity *versus* scattering vector (*q*)/Å. *C* and *D*, a plot of the relative protein concentration *versus* the sedimentation coefficient corrected for water at 20 °C ($s_{20,w}$) of the L4-MRE11 heterotetramer (*C*) or the L4-MRE11 heterotetramer in the presence of DNA (*D*) and in the presence (*green*) or the absence (*blue*) of ATP (Mg^{2+}). *Red* indicates the ($s_{20,w}$) for 40-bp double-stranded DNA in the absence of protein. *E* and *F*, the open complex binds best to DNA. L4 or L4-MRE11 binding to a 2 nM 5′-FITC-labeled single strand of 40 nucleotides (supplemental sequences, 40 bot-FITC) or double-stranded DNA of 40 base pairs (supplemental sequences, 40 bot and 40 top) was measured by fluorescence anisotropy. Shown is anisotropy *versus* protein concentration. DNA was incubated with the indicated amount of protein (expressed as concentration of ATP binding sites) for 5 min at 25 °C in a 20-μl reaction volume. The samples contained 5 mM $MgCl_2$ or $MnCl_2$ and 200 μM ATP as indicated. Anisotropy was measured in a TECAN plate reader using excitation and emission wavelengths of 470 and 522 nm, respectively. Data were fit (*solid lines*) to the Langmuir isotherm.

nuclease activity of MRE11 under these conditions (compare Fig. C and Fig. 5*E*). To test whether RAD50 ATPase activity promoted the MRE11 exonuclease activity, we blocked it using ATPγS (Fig. 5*E*). Unexpectedly, the specific activity (k_{cat}/K_m) of the L4-MRE11 exonuclease activity was suppressed around 2-fold by the addition of ATPγS (Mg^{2+} and Mn^{2+}) relative to the addition of ATP (Mg^{2+} and Mn^{2+}) (Fig. 5*E*, supplemental Table SIII) and about 5-fold relative to MRE11 alone (compare Fig. 5, *D* and *E*, supplemental Table SIII). Thus, the level of exonuclease activity of RAD50-MRE11 depended on ATP

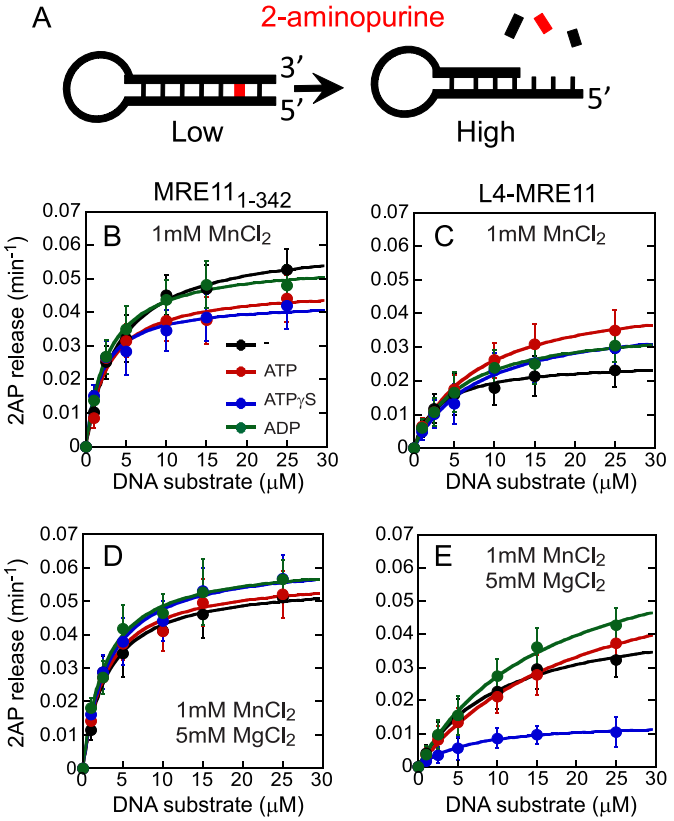

FIGURE 5. **RAD50 ATP hydrolysis prevents shutdown of the MRE11 exonuclease activity.** *A*, shown is a schematic representation of the DNA hairpin substrate used in the assays. *B*, the exonuclease reactions comprise 2 μM $MRE11_{1-342}$ or L4-MRE11 protein, 200 μM nucleotide, and the indicated concentrations of 2-AP DNA substrate. Samples were incubated at 55 °C. After 2, 4, 6, 10, 15, and 20 min, 20-μl aliquots were removed and quenched, and the released 2-AP was measured in TECAN plate reader using excitation and emission wavelength of 310 and 375 nm, respectively. The intensities used to determine the turnover number/min/protein monomer were always measured in the linear range of a calibration curve from the fluorescence intensity of free 2-amino purine. Data were fitted (*solid lines*) using Michaelis-Menten equation. The added ions are indicated (*B–E*).

hydrolysis but not by a canonical stimulation mechanism. Rather, ATP hydrolysis prevented shutdown of MRE11 exonuclease activity. Because it was suppressed by ATPγS only under conditions of active hydrolysis (compare Fig. 5, *C* and *E*), these findings implied that maintenance of exonuclease activity depended on the open conformation. Consistent with a regulatory role for ATP hydrolysis in maintaining the open complex, the exonuclease activity was highest when L4-MRE11 was ADP-bound (Fig. 5*E*).

To determine the extent to which ATP hydrolysis regulated MRE11 exonuclease activity, we measured the catalytic rate of ATP hydrolysis relative to the rate of exonuclease activity. RAD50 was a weak ATPase (Fig. 3*D*), with a maximum rate no greater than 15 molecules of ATP per minute (per ATP binding site) under optimum conditions. ATP hydrolysis did not change when RAD50-MRE11 was bound to DNA. However, the rate of ATP turnover in the L4 subunits of L4-MRE11 was >100-fold higher than the k_{cat} of the MRE11 exonuclease (compare Fig. 3*D* and supplemental Table SIII). Thus, ATP hydrolysis did not limit the velocity of nucleotide release from the 3′ end.

ATP Hydrolysis in RAD50 Switches MRE11 from Exonuclease to Endonuclease—We next evaluated the effect of nucleotide-dependent structural dynamics of the endonuclease activity of MRE11 in the presence of Mg^{2+} and Mn^{2+}. To measure the endonuclease activity, we developed a second DNA template in which the endo- and exonucleotide could be visualized individually or simultaneously by adjusting the solution conditions (Fig. 6*A*). The 59-nucleotide template folded back to form a duplex region of 22 base pairs, a 3-nucleotide loop, and 6 nucleotide ssDNA overhangs on both the 3′ and the 5′ end. The MRE11 endonuclease activity is highest on ssDNA at protruding 3′ and 5′ ends and 3′ branches (27–29). Thus, the hairpin template was ^{32}P-labeled on the 5′ terminus, and the endonuclease activity was measured by the reduction in the length of the incision product after resolution on PAGE gels (Fig. 6*B*).

For L4-MRE11, we anticipated that if the MRE11 endonuclease were active, then it would remove either of the two arms of the template, one of which would retain the ^{32}P-label (Fig. 6, *A* and *B*, *red arrows*). Indeed, when we incubated L4-MRE11 with the DNA substrate in the presence of both ATP (Mn^{2+}) and ATP (Mg^{2+}), we observed a doublet band corresponding to endonucleolytic removal of the overhang at the junction between the dsDNA and ssDNA and 1–2 nucleotides from the end (*lane 3*, Fig. 6*B*, *red arrows*). The endonucleolytic function of MRE11 was specific to MRE11 and required ATP binding. No incision product was observed after the addition of ATP in the absence of L4-MRE11 (*lane 1*, Fig. 6*B*) or for the L4-MRE11 complex without ATP (*lane 2*, Fig. 6*B*). Furthermore, no incision activity was observed for $MRE11_{1-342}$ and L4-MRE11 in the absence of Mn^{2+} under any conditions tested (*lanes 10* and *11*, Fig. 6*B*).

In contrast to the exonuclease activity of MRE11, however, ATP hydrolysis in the subunits of L4 was not required for endonuclease activity of MRE11. When ATPγS was the added nucleotide, L4-MRE11 generated an incision product that was five-six nucleotides shorter than the original template and more specific for ssDNA/dsDNA junction (*lane 4*, Fig. 6*B*). No incision product was detected when ADP was the added nucleotide (*lane 5*, Fig. 6*B*), conditions under which the exonuclease activity was highest.

We repeated the analysis with MRE11 alone in the absence of L4. Indeed, we observed promiscuous exonuclease and endonuclease products of $MRE11_{1-342}$ (*lanes 6–9*, Fig. 6*B*), consistent with loss of its inhibition by RAD50 (Fig. 5*C*). Thus, regulation of the endo- and exonuclease activities of MRE11 depended on the presence of L4. Moreover, the exonuclease and endonuclease functions depended differently on the open and closed complexes of L4-MRE11. ATP hydrolysis shifted equilibrium toward the open complex, a condition under which the exonuclease activity of MRE11 was maintained. In contrast, the endonuclease activity of MRE11 depended only on ATP binding, which tended to close the RAD50-MRE11 complex.

To further test the dependence of MRE11 endonuclease activity on the ATP dynamics of RAD50, we repeated the assay in the presence of Mn^{2+} alone or together with Mg^{2+} using a series of templates comprising 3′ overhangs, 5′ overhangs, or blunt ends (supplemental Fig. S4). Each of these templates was labeled with ^{32}P on the 5′ end (supplemental Fig. S4*A*). Within

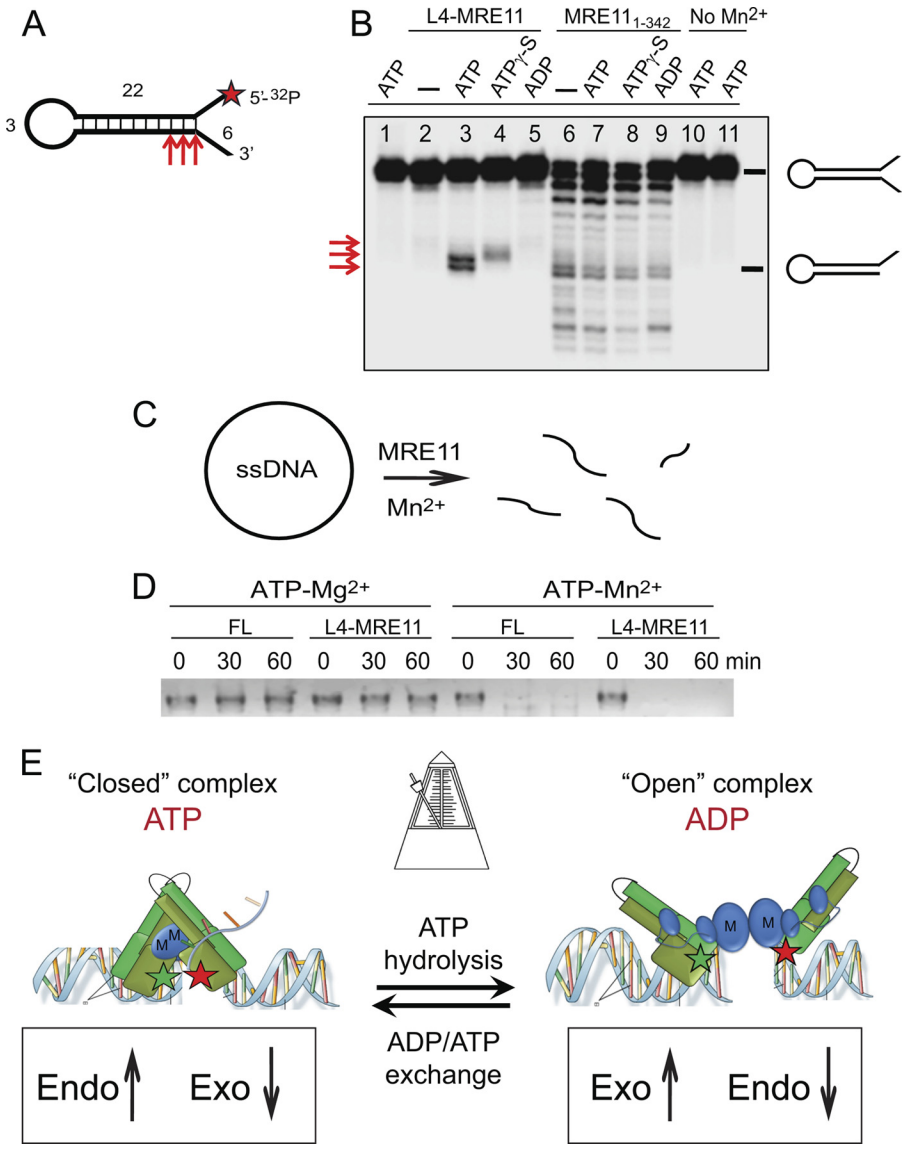

FIGURE 6. **ATP binding stimulates endonuclease activity of the RAD50-MRE11 complex.** *A*, shown is a schematic representation of the DNA hairpin substrate used in the endonuclease assays. The *asterisk* marks position of the ^{32}P label. The *numbers* indicate the nucleotide length in each segment of the template. *B*, assays contained 2 μM MRE11 or L4-MRE11 protein, 200 μM nucleotide, 5 mM concentrations of both $MgCl_2$ and $MnCl_2$, and ~1 nM DNA substrate (10,000 cpm). Reactions were incubated at 55 °C for 2 h and stopped with gel loading buffer, and the products were resolved by 12% urea-PAGE followed by phosphorimaging. *Lane 1*, templates with ATP but no L4-MRE11; *lane 2*, L4-MRE11 with no nucleotide; *lane 3*, L4-MRE11 and ATP; *lane 4*, L4-MRE11 and ATPγS; *lane 5*, L4-MRE11 and ADP; *lane 6*, $MRE11_{1-342}$ and no nucleotide; *lanes 7–9*, $MRE11_{1-342}$ with ATP, ATPγS, and ADP, respectively; *lane 10*, ATP and L4-MRE11 and no manganese; *lane 11*, $MRE11_{1-342}$ and ATP no manganese. Migration of the endonuclease products is shown on the *right*. *Red arrows* (*left*) are reaction products corresponding to *A*. *C*, shown is an endonuclease assay using plasmid DNA. The assays contained 2 μg of ss plasmid, 1 μM FL or L4-MRE11 protein, and 1 mM ATP incubated with 5 mM concentrations of the indicated cation. Both full-length RAD50-MRE11 (*FL*) and L4-MRE11 were used, as indicated. Samples were taken at 0, 30, and 60 min. Disappearance of the band indicates incision. *E*, shown is a switching model for RAD50-MRE11. Butterfly-like opening and closing act as a metronome for switching the nucleolytic activity of MRE11 between exonuclease and endonuclease functions. Nucleotide exchange resets the clock.

60 min the single-stranded tails were removed by MRE11 endonuclease activity in templates containing the 3′ overhang whether or not Mg^{2+} was present in the reaction. Each reaction product was shorter by five-six nucleotides, consistent with incision at the ssDNA-dsDNA junction. As a control, we followed the reaction product of a 5′ overhang, which cannot be processed by the MRE11 exonuclease function. Indeed, consistent with an endonuclease activity, incision resulted in loss of the 5′ end ssDNA tail, and the 5′ ^{32}P-labeled product was no longer observed. No activity was observed in the absence of ATP. Thus, the endonuclease activity of MRE11 did not require ATP hydrolysis in the RAD50 subunits.

In a final set of experiments, we measured the endonuclease activity on ss plasmid DNA using both the FL and L4-MRE11 proteins (Fig. 6*C*). Due to its circular nature, any incision event will arise from endonucleolytic activity on the plasmid DNA. The linearized template was detected by ethidium staining after resolution on agarose gels. Indeed, ATP (Mn^{2+}) addition to either L4-MRE11 or FL resulted in loss of the DNA template within 30 min (Fig. 6*D*, ATP-Mn^{2+}). In the absence of Mn^{2+}, no degradation was observed when ATP (Mg^{2+}) was the added nucleotide (Fig. 6*D*, *ATP-*Mg^{2+}). Thus, the endonuclease activity of RAD50-MRE11 depended on ATP binding but not on its hydrolysis. Collectively, these results implied that opening and

closing of RAD50-MRE11 complexes imparted distinct physiological roles that fundamentally converted the nucleolytic function of MRE11 between exonuclease and endonuclease functions. ATP hydrolysis served as a switch between these two activities.

DISCUSSION

RAD50 forms a tight complex with MRE11, yet the molecular mechanism by which RAD50 and MRE11 communicate to orchestrate damage detection is poorly understood. Moreover, ATP regulates MRE11 functions, but the role of ATP binding in discriminating DNA end processing and the role of ATP hydrolysis are unknown. We report here that RAD50 coordinates these two activities of MRE11 by ATP-dependent structural rearrangements and a remarkable ability to switch MRE11 nucleolytic activity. Continuous cycles of ATP binding and ATP hydrolysis impart a "butterfly" movement that opens and closes the RAD50-MRE11 complex (Fig. 6*E*). ATP binding shifts the equilibrium to closed conformation, in which MRE11 is an endonuclease. ATP hydrolysis shifts the equilibrium to the open state in which MRE11 is an exonuclease (Fig. 6*E*). We find that ATP hydrolysis acts as a biological switch that converts the MRE11 endonuclease into an exonuclease (Fig. 6*E*). Although conformational changes in proteins commonly play regulatory roles, the findings presented here are among the first examples where structural alterations are used to entirely change the function of the protein.

ATP-dependent nuclease switching provides a plausible mechanism and critical insight into how a single RAD50-MRE11 complex is able to coordinate DNA repair, DNA end recognition, and decision points for directing repair to HR, non-homologous end joining, or microhomology-mediated end joining repair pathways.

RAD50 Provides Check and Balance System for MRE11-dependent DNA Repair—RAD50 is exquisitely designed to act as a critical "check and balance" system to coordinate the DNA repair function of MRE11. Arguably, the most important modular function of RAD50 is to avoid unregulated activity of MRE11. In the absence of RAD50, MRE11 behaves like a "runaway train" and operates indiscriminately and simultaneously on both ssDNA and dsDNA (Fig. 6*B*). Unregulated MRE11-mediated activity predicts an increase in the demand for double strand break repair, but recruitment of unregulated MRE11 itself would cause more breaks. Thus, the interaction of RAD50 with MRE11 is poised to minimize toxic and futile cycles of nuclease activity. Importantly, suppression of the MRE11 nuclease by RAD50 is its only nucleotide-independent function (Fig. 5). Thus, the repressive action of RAD50 provides an intrinsic gate-keeping function and a global check of MRE11 activity. Interestingly, a negative regulatory function of RAD50 protein was recently observed in another archaeal species *Methanococcus jannaschii* (26). Thus, our results imply that repression of MRE11 is likely to be a common function of RAD50.

The "balance" for the DNA repair activity of MRE11 is provided by the nucleotide-dependent properties of RAD50. In the ADP-bound state, the endonuclease activity of RAD50 is lost, and the exonuclease activity is at its maximum (Figs. 5 and 6, *A* and *B*). Because ATP and ADP bound in RAD50 subunits are in rapid exchange with solution nucleotides (Fig. 1*G*), ATP replaces ADP, and the endonucleolytic form of MRE11 is active again. Thus, opening and closing of RAD50-MRE11 are reminiscent of a DNA clamp, which characterizes other DNA binding members of the ABC-ATPase superfamily (40, 53, 54).

We find that RAD50-MRE11 most frequently exists as an ATP-bound endonuclease in the closed conformation. However, as judged by its biochemical properties, limiting the exonuclease activity of MRE11 appears to be the most crucial role of RAD50 nucleotide dynamics. Indeed, in the absence of ATP hydrolysis, we find that the exonuclease plummets nearly 5-fold relative to the MRE11 alone (Fig. 5). Under these conditions, MRE11 would be unable to generate microhomology domains or to remove blocked ends for successful recombination or end joining (supplemental Fig. S5). In this regard, ATP hydrolysis is not a canonical "activator" of MRE11 but is designed to avoid loss of its exonuclease function and maintain it at a useful level. The activity of the MRE11 as an exonuclease is maximal when RAD50 is an ADP-bound complex and the endonuclease function is suppressed (Figs. 5 and 6). However, the rate of ATP hydrolysis exceeds the rate of MRE11 exonuclease activity, and rapid ADP-ATP exchange quickly returns RAD50-MRE11 to a closed ATP-bound state. Collectively, the nucleotide dynamics in the RAD50 subunits provide a brief window within which MRE11 can function as the exonuclease and strictly limits the number of nucleotides released from the 3′ end.

Model for Switching-directed Pathway Choice—The RAD50-MRE11-Nbs1 complex has been implicated in every aspect of DSB processing from the initial detection to the choice among pathways for repair. Based on the nucleotide dynamics of RAD50, we propose a testable model in which the structural changes integrate the nucleolytic processing of MRE11 and the tethering functions of RAD50-MRE11 to direct pathway choice. MRE11 has both endo- and an exonuclease activity *in vitro*, but whether these functions are coordinated remains enigmatic. However, the continuous MRE11 exo-endo cycle poises MRE11 for ordered and sequential nuclease functions in rapid succession. Opening and closing of RAD50-MRE11 is independent of DNA binding. However, RAD50-MRE11 binds best to DNA in an open exonuclease-active form, and ADP-bound RAD50-MRE11 has a preference for ssDNA overhang in that state (Fig. 6*E*). The rapid exchange of ADP for ATP exchange results in closing of ATP-bound RAD50-MRE11 around the ssDNA or dsDNA junction, yielding endonucleolytic incision of the overhang and production of a blunt end (Fig. 6*E*).

ATP hydrolysis promotes a second opening event, and in the open state, RAD50-MRE11 adopts extended conformation and either dissociates or is poised to span between DNA ends as a tethering bridge. At flush ends, the open RAD50-MRE11 is competent for 3′ to 5′ MRE11 exonuclease activity and, after nibbling into the 3′ end, likely hands the ends to Sae2/CtIp for 5′ to 3′ resection and successful HR (6, 31). RAD50-MRE11 has a dsDNA melting activity (29), which presumably aids in 3′ to 5′ exonuclease activity.

Because both the endo- and exonuclease activities of MRE11 occur in the presence of ATP, RAD50-MRE11 is unlikely to

efficiently discriminate among hairpin opening, ssDNA endonuclease, dsDNA exonuclease, and 5′ dsDNA endonuclease *in vitro*. However, RAD50-MRE11 affinity for particular DNA ends provides a plausible means for the precise roles for RAD50-MRE11 in double strand break repair *in vivo*. RAD50-MRE11 does not efficiently process 3′ overhangs or hairpin DNA, but it binds to those substrates with significant affinity (27). In these cases we envision a mechanism by which MRE11-RAD50 acts as a scaffold and recruits DNA-PK (55) (or another suitable component of the repair machinery) to complete end processing. The ability of RAD50-MRE11 to process a particular type of end provides a plausible and simple driver to direct pathway choice. The rapid opening and closing and nuclease switching ensures that the complex broadly recognizes most DNA broken ends but uses end recognition to distinguish between direct nucleolytic processing *versus* scaffolding and recruitment. Whatever the detailed mechanisms, RAD50-MRE11 is a "first responder" for DSBs. The structural rearrangements of RAD50-MRE11 complex and its ability to switch nucleolytic functions poise it for integration of ATP dynamics, nucleolytic processing, and pathway selection.

REFERENCES

1. Williams, G. J., Lees-Miller, S. P., and Tainer, J. A. (2010) Mre11-Rad50-Nbs1 conformations and the control of sensing, signaling, and effector responses at DNA double-strand breaks. *DNA Repair* **9,** 1299–1306
2. Paull, T. T. (2010) Making the best of the loose ends. Mre11-Rad50 complexes and Sae2 promote DNA double-strand break resection. *DNA Repair* **9,** 1283–1291
3. Stracker, T. H., and Petrini, J. H. (2011) The MRE11 complex. Starting from the ends. *Nat. Rev. Mol. Cell Biol.* **12,** 90–103
4. Mimitou, E. P., and Symington, L. S. (2011) DNA end resection. Unraveling the tail. *DNA Repair* **10,** 344–348
5. Polo, S. E., and Jackson, S. P. (2011) Dynamics of DNA damage response proteins at DNA breaks. A focus on protein modifications. *Genes Dev.* **25,** 409–433
6. Mimitou, E. P., and Symington, L. S. (2009) DNA end resection. Many nucleases make light work. *DNA Repair* **8,** 983–995
7. Chen, L., Trujillo, K., Ramos, W., Sung, P., and Tomkinson, A. E. (2001) Promotion of Dnl4-catalyzed DNA end-joining by the Rad50-Mre11-Xrs2 and Hdf1-Hdf2 complexes. *Mol. Cell* **8,** 1105–1115
8. Clerici, M., Mantiero, D., Guerini, I., Lucchini, G., and Longhese, M. P. (2008) The Yku70-Yku80 complex contributes to regulate double-strand break processing and checkpoint activation during the cell cycle. *EMBO Rep.* **9,** 810–818
9. Lee, S. E., Moore, J. K., Holmes, A., Umezu, K., Kolodner, R. D., and Haber, J. E. (1998) *Saccharomyces* Ku70, mre11/rad50, and RPA proteins regulate adaptation to G_2/M arrest after DNA damage. *Cell* **94,** 399–409
10. Lewis, L. K., Storici, F., Van Komen, S., Calero, S., Sung, P., and Resnick, M. A. (2004) Role of the nuclease activity of *Saccharomyces cerevisiae* Mre11 in repair of DNA double-strand breaks in mitotic cells. *Genetics* **166,** 1701–1713
11. Palmbos, P. L., Wu, D., Daley, J. M., and Wilson, T. E. (2008) Recruitment of *Saccharomyces cerevisiae* Dnl4-Lif1 complex to a double-strand break requires interactions with Yku80 and the Xrs2 FHA domain. *Genetics* **180,** 1809–1819
12. Lisby, M., Barlow, J. H., Burgess, R. C., and Rothstein, R. (2004) Choreography of the DNA damage response. Spatiotemporal relationships among checkpoint and repair proteins. *Cell* **118,** 699–713
13. Buis, J., Wu, Y., Deng, Y., Leddon, J., Westfield, G., Eckersdorff, M., Sekiguchi, J. M., Chang, S., and Ferguson, D. O. (2008) Mre11 nuclease activity has essential roles in DNA repair and genomic stability distinct from ATM activation. *Cell* **135,** 85–96
14. Williams, R. S., Moncalian, G., Williams, J. S., Yamada, Y., Limbo, O., Shin, D. S., Groocock, L. M., Cahill, D., Hitomi, C., Guenther, G., Moiani, D., Carney, J. P., Russell, P., and Tainer, J. A. (2008) Mre11 dimers coordinate DNA end bridging and nuclease processing in double-strand break repair. *Cell* **135,** 97–109
15. Costanzo, V., Robertson, K., Bibikova, M., Kim, E., Grieco, D., Gottesman, M., Carroll, D., and Gautier, J. (2001) Mre11 protein complex prevents double-strand break accumulation during chromosomal DNA replication. *Mol. Cell* **8,** 137–147
16. Trenz, K., Smith, E., Smith, S., and Costanzo, V. (2006) ATM and ATR promote Mre11-dependent restart of collapsed replication forks and prevent accumulation of DNA breaks. *EMBO J.* **25,** 1764–1774
17. Wen, Q., Scorah, J., Phear, G., Rodgers, G., Rodgers, S., and Meuth, M. (2008) A mutant allele of MRE11 found in mismatch repair-deficient tumor cells suppresses the cellular response to DNA replication fork stress in a dominant negative manner. *Mol. Biol. Cell* **19,** 1693–1705
18. Mirzoeva, O. K., and Petrini, J. H. (2001) DNA damage-dependent nuclear dynamics of the Mre11 complex. *Mol. Cell Biol.* **21,** 281–288
19. Nakada, D., Matsumoto, K., and Sugimoto, K. (2003) ATM-related Tel1 associates with double-strand breaks through an Xrs2-dependent mechanism. *Genes Dev.* **17,** 1957–1962
20. Falck, J., Coates, J., and Jackson, S. P. (2005) Conserved modes of recruitment of ATM, ATR, and DNA-PKcs to sites of DNA damage. *Nature* **434,** 605–611
21. Mantiero, D., Clerici, M., Lucchini, G., and Longhese, M. P. (2007) Dual role for *Saccharomyces cerevisiae* Tel1 in the checkpoint response to double-strand breaks. *EMBO Rep.* **8,** 380–387
22. Olson, E., Nievera, C. J., Lee, A. Y., Chen, L., and Wu, X. (2007) The Mre11-Rad50-Nbs1 complex acts both upstream and downstream of ataxia telangiectasia mutated and Rad3-related protein (ATR) to regulate the S-phase checkpoint after UV treatment. *J. Biol. Chem.* **282,** 22939–22952
23. Carson, C. T., Orazio, N. I., Lee, D. V., Suh, J., Bekker-Jensen, S., Araujo, F. D., Lakdawala, S. S., Lilley, C. E., Bartek, J., Lukas, J., and Weitzman, M. D. (2009) Mislocalization of the MRN complex prevents ATR signaling during adenovirus infection. *EMBO J.* **28,** 652–662
24. Sun, Y., Jiang, X., and Price, B. D. (2010) Tip60; connecting chromatin to DNA damage signaling. *Cell Cycle* **9,** 930–936
25. Hopfner, K. P., Karcher, A., Shin, D., Fairley, C., Tainer, J. A., and Carney, J. P. (2000) Mre11 and Rad50 from *Pyrococcus furiosus*. Cloning and biochemical characterization reveal an evolutionarily conserved multiprotein machine. *J. Bacteriol.* **182,** 6036–6041
26. Lim, H. S., Kim, J. S., Park, Y. B., Gwon, G. H., and Cho, Y. (2011) Crystal structure of the Mre11-Rad50-ATPγS complex. Understanding the interplay between Mre11 and Rad50. *Genes Dev.* **25,** 1091–1104
27. Paull, T. T., and Gellert, M. (1998) The 3′ to 5′ exonuclease activity of Mre 11 facilitates repair of DNA double-strand breaks. *Mol. Cell* **1,** 969–979
28. Trujillo, K. M., and Sung, P. (2001) DNA structure-specific nuclease activities in the *Saccharomyces cerevisiae* Rad50-Mre11 complex. *J. Biol. Chem.* **276,** 35458–35464
29. Paull, T. T., and Gellert, M. (1999) Nbs1 potentiates ATP-driven DNA unwinding and endonuclease cleavage by the Mre11-Rad50 complex. *Genes Dev.* **13,** 1276–1288
30. Lengsfeld, B. M., Rattray, A. J., Bhaskara, V., Ghirlando, R., and Paull, T. T. (2007) Sae2 is an endonuclease that processes hairpin DNA cooperatively with the Mre11-Rad50-Xrs2 complex. *Mol. Cell* **28,** 638–651
31. Nicolette, M. L., Lee, K., Guo, Z., Rani, M., Chow, J. M., Lee, S. E., and Paull, T. T. (2010) Mre11-Rad50-Xrs2 and Sae2 promote 5′ strand resection of DNA double-strand breaks. *Nat. Struct. Mol. Biol.* **17,** 1478–1485
32. Huertas, P., and Jackson, S. P. (2009) Human CtIP mediates cell cycle control of DNA end resection and double-strand break repair. *J. Biol. Chem.* **284,** 9558–9565
33. Williams, R. S., Dodson, G. E., Limbo, O., Yamada, Y., Williams, J. S., Guenther, G., Classen, S., Glover, J. N., Iwasaki, H., Russell, P., and Tainer, J. A. (2009) Nbs1 flexibly tethers Ctp1 and Mre11-Rad50 to coordinate DNA double-strand break processing and repair. *Cell* **139,** 87–99
34. Trujillo, K. M., Roh, D. H., Chen, L., Van Komen, S., Tomkinson, A., and Sung, P. (2003) Yeast xrs2 binds DNA and helps target rad50 and mre11 to DNA ends. *J. Biol. Chem.* **278,** 48957–48964

35. Alani, E., Subbiah, S., and Kleckner, N. (1989) The yeast RAD50 gene encodes a predicted 153-kD protein containing a purine nucleotide binding domain and two large heptad-repeat regions. *Genetics* **122,** 47–57
36. Sharples, G. J., and Leach, D. R. (1995) Structural and functional similarities between the SbcCD proteins of *Escherichia coli* and the RAD50 and MRE11 (RAD32) recombination and repair proteins of yeast. *Mol. Microbiol.* **17,** 1215–1217
37. Hopfner, K. P., Karcher, A., Craig, L., Woo, T. T., Carney, J. P., and Tainer, J. A. (2001) Structural biochemistry and interaction architecture of the DNA double-strand break repair Mre11 nuclease and Rad50-ATPase. *Cell* **105,** 473–485
38. Hopfner, K. P., Karcher, A., Shin, D. S., Craig, L., Arthur, L. M., Carney, J. P., and Tainer, J. A. (2000) Structural biology of Rad50 ATPase. ATP-driven conformational control in DNA double-strand break repair and the ABC-ATPase superfamily. *Cell* **101,** 789–800
39. Hirano, T. (2005) SMC proteins and chromosome mechanics. From bacteria to humans. *Philos. Trans. R. Soc. Lond B. Biol. Sci.* **360,** 507–514
40. Rees, D. C., Johnson, E., and Lewinson, O. (2009) ABC transporters. The power to change. *Nat. Rev. Mol. Cell Biol.* **10,** 218–227
41. Lammens, K., Bemeleit, D. J., Möckel, C., Clausing, E., Schele, A., Hartung, S., Schiller, C. B., Lucas, M., Angermüller, C., Söding, J., Strässer, K., and Hopfner, K. P. (2011) The Mre11-Rad50 structure shows an ATP-dependent molecular clamp in DNA double-strand break repair. *Cell* **145,** 54–66
42. Williams, G. J., Williams, R. S., Williams, J. S., Moncalian, G., Arvai, A. S., Limbo, O., Guenther, G., SilDas, S., Hammel, M., Russell, P., and Tainer, J. A. (2011) ABC ATPase signature helices in Rad50 link nucleotide state to Mre11 interface for DNA repair. *Nat. Struct. Mol. Biol.* **18,** 423–431
43. Alani, E., Padmore, R., and Kleckner, N. (1990) Analysis of wild-type and rad50 mutants of yeast suggests an intimate relationship between meiotic chromosome synapsis and recombination. *Cell* **61,** 419–436
44. Nairz, K., and Klein, F. (1997) mre11S, a yeast mutation that blocks double-strand break processing and permits nonhomologous synapsis in meiosis. *Genes Dev.* **11,** 2272–2290
45. Putnam, C. D., Hammel, M., Hura, G. L., and Tainer, J. A. (2007) X-ray solution scattering (SAXS) combined with crystallography and computation. Defining accurate macromolecular structures, conformations, and assemblies in solution. *Q Rev. Biophys.* **40,** 191–285
46. Hura, G. L., Menon, A. L., Hammel, M., Rambo, R. P., Poole, F. L., 2nd, Tsutakawa, S. E., Jenney, F. E., Jr., Classen, S., Frankel, K. A., Hopkins, R. C., Yang, S. J., Scott, J. W., Dillard, B. D., Adams, M. W., and Tainer, J. A. (2009) Robust, high throughput solution structural analyses by small angle X-ray scattering (SAXS). *Nat. Methods* **6,** 606–612
47. Svergun, D. I. (1992) Determination of the regularization parameter in indirect-transform methods using perceptual criteria. *J. Appl. Crystallogr.* **25,** 495–503
48. Demeler, B., and van Holde, K. E. (2004) Sedimentation velocity analysis of highly heterogeneous systems. *Anal. Biochem.* **335,** 279–288
49. Owen, B. A., Yang, Z., Lai, M., Gajek, M., Badger, J. D., 2nd, Hayes, J. J., Edelmann, W., Kucherlapati, R., Wilson, T. M., and McMurray, C. T. (2005) (CAG)(n)-hairpin DNA binds to Msh2-Msh3 and changes properties of mismatch recognition. *Nat. Struct. Mol. Biol.* **12,** 663–670
50. Owen, B. A., H Lang, W., and McMurray, C. T. (2009) The nucleotide binding dynamics of human MSH2-MSH3 are lesion-dependent. *Nat. Struct. Mol. Biol.* **16,** 550–557
51. Cao, W., and Demeler, B. (2005) Modeling analytical ultracentrifugation experiments with an adaptive space-time finite element solution of the Lamm equation. *Biophys. J.* **89,** 1589–1602
52. Shuck, P. (2010) Diffusion in the reaction boundary of rapidly interacting macromolecules in sedimentation velocity. *Biophys. J.* **98,** 2741–2747
53. Moncalian, G., Lengsfeld, B., Bhaskara, V., Hopfner, K. P., Karcher, A., Alden, E., Tainer, J. A., and Paull, T. T. (2004) The rad50 signature motif. Essential to ATP binding and biological function. *J. Mol. Biol.* **335,** 937–951
54. Kinoshita, E., van der Linden, E., Sanchez, H., and Wyman, C. (2009) RAD50, an SMC family member with multiple roles in DNA break repair. How does ATP affect function? *Chromosome Res.* **17,** 277–288
55. Shrivastav, M., De Haro, L. P., and Nickoloff, J. A. (2008) Regulation of DNA double-strand break repair pathway choice. *Cell Res.* **18,** 134–147